STRAHL modeling of iron impurity transport with on- and off-axis heating during the first divertor campaign on Wendelstein 7-X

Peter Traverso[1]

N. Pablant[2], A. Langenberg[3], Th. Wegner[3], B. Geiger[4], B. Buttenschön[3], H. M. Smith[3], R. Burhenn[3], D. Zhang[3], J. Schmitt[1], J. Kring[1], D. Maurer[1], & W7-X Team

[1]Auburn University, [2]PPPL, [3]IPP Greifswald Germany, [4]University of Wisconsin

X-ray Imaging Crystal Spectrometer (XICS) as a plasma diagnostic

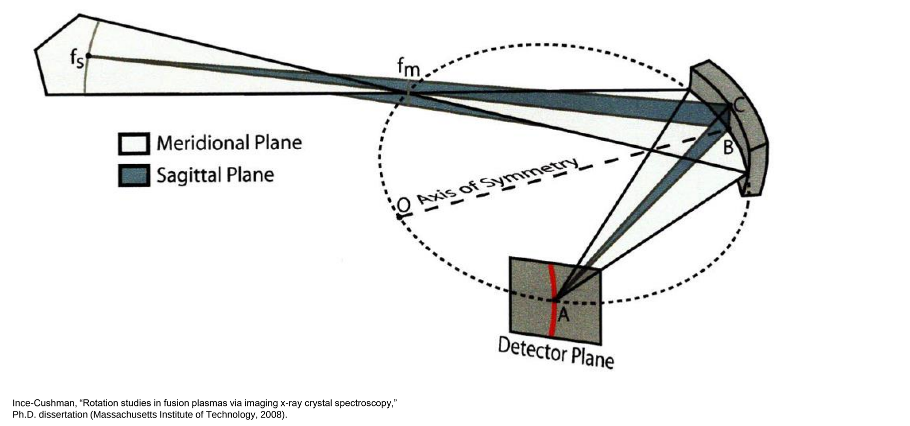

- Measures impurity line radiation from the highly charged states of medium Z materials
- Crystal astigmatism yields a 1-D image of the plasma
- Amounts of medium Z materials required for a measurement are non-perturbative

- Ion temperature (T_i) : line width
- Electron temperature (T_e) : ratio of specific lines
- Ion Flow velocity ($v_\perp$) : line shift
- Impurity density ($n_{impurity}$) : line intensity

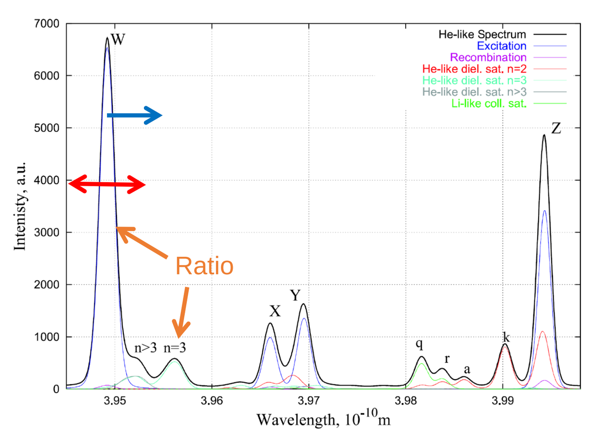

He-like Argon spectra (Ar XVII)

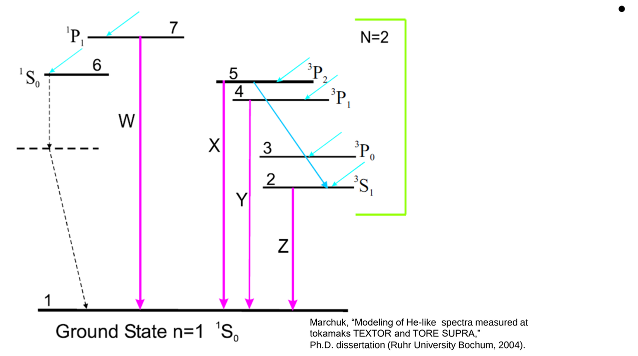

- Atomic physics of He-like line emission leveraged to create accurate spectral model
- Line integrated plasma parameters can be inferred from spectral fit
- Utilizing the 1-D spectral image, tomographic inversions can yield profile information

- Fast time resolution with coupled spatial information from 1-D image make this an ideal diagnostic for studying impurity transport

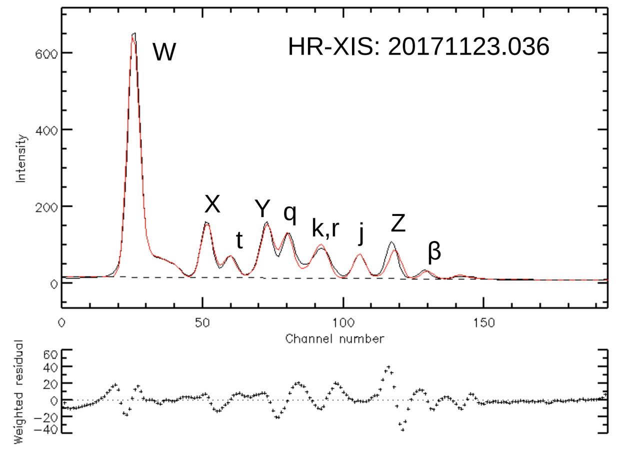

He-like Iron spectra (Fe XXV)

Transport diagnostics on W7-X: XICS, HR-XIS, HEXOS, & LBO

XICS and HR-XIS capabilities

Spectrometer Properties		Physics Quantity
Spatial Resolution	2.0 cm	
Throughput	??	$n_Z / n_e > 5\times10^{-5}$
Dispersion	2.4×10^{-3} Å/mm 4.2×10^{-4} Å/pixel	$\Delta T_i = \pm 80$ eV (1 pixel 172 µm)
Line Position	5×10^{-5} Å	$\Delta v = \pm 2.5$ km/s
Time Res.	2 - 5 ms	

System	Crystal (Cut)	Bragg Angle /°	Impurity	Status
HR-XIS	Quartz (-110)	51.88	Si^{12+}	√
	Quartz(11-20)	54.04	Ar^{16+}	√
	Si (311)	53.22	Ti^{20+}	√
	Ge (422)	53.61	Fe^{24+}	√
	Ge (440)	52.95	Ni^{26+}	√
	Si (531)	54.00	Cu^{27+}	√
	Ge (533)	51.96	W^{64+}	×
XICS	Quartz(11-20)	54.04	Ar^{16+}	√
	Quartz(10-12)	49.58	Ar^{17+} Fe^{24+} Mo^{32+}	√

HR-XIS system

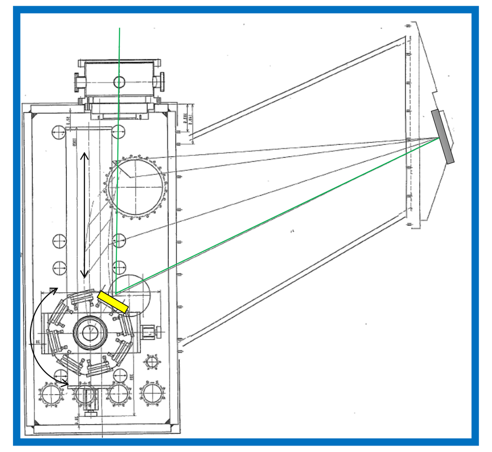

Ar^{16+}

Sightlines

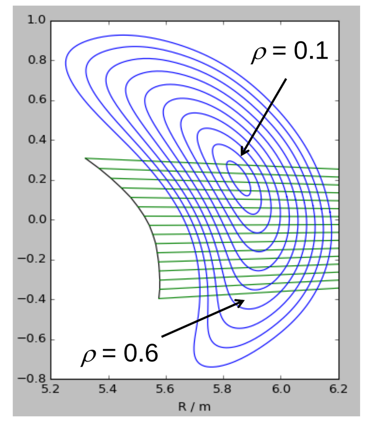

HEXOS: XUV Spectroscopy

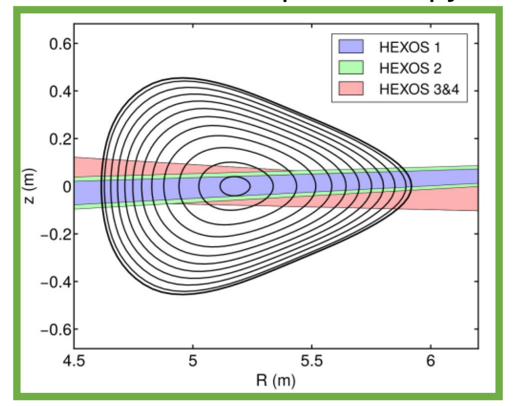

- 4 individual spectrometers
- Complete spectral coverage 2.4 nm to 161.1nm
- 1 kHz sample rate

XICS system

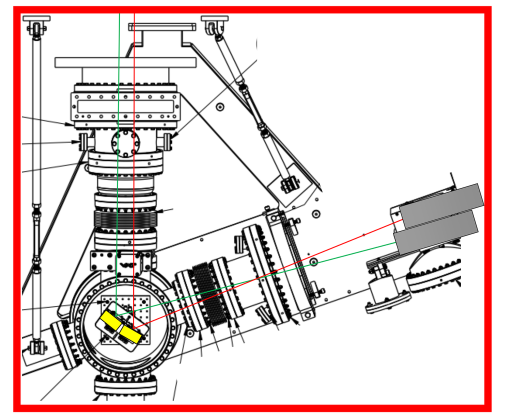

Ar^{17+} Ar^{16+}

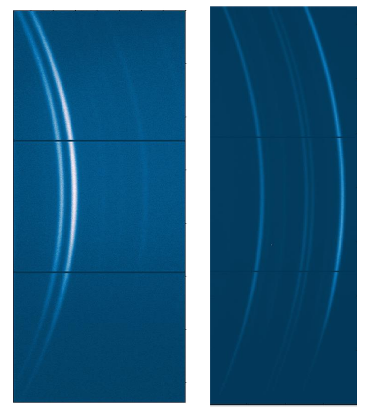

Sightlines

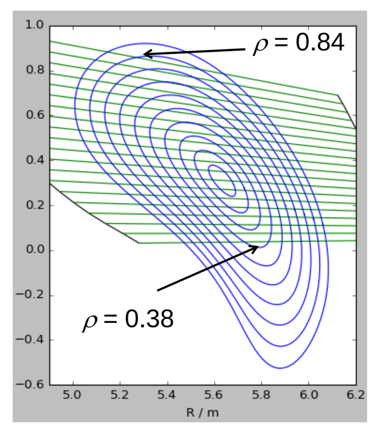

Top View W7-X

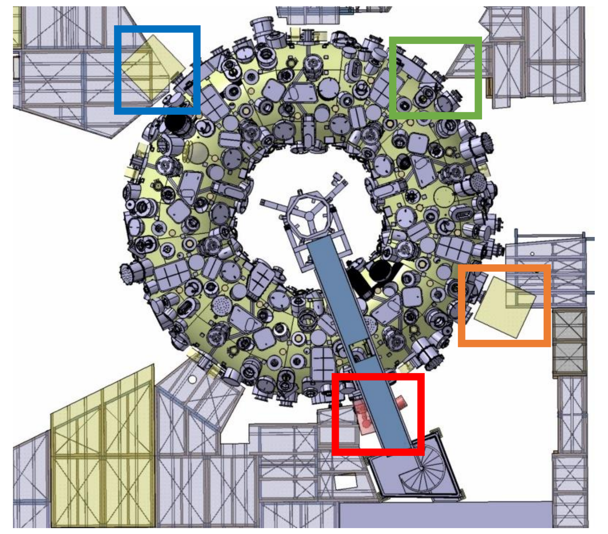

Laser Blow Off (LBO): Impurity injection

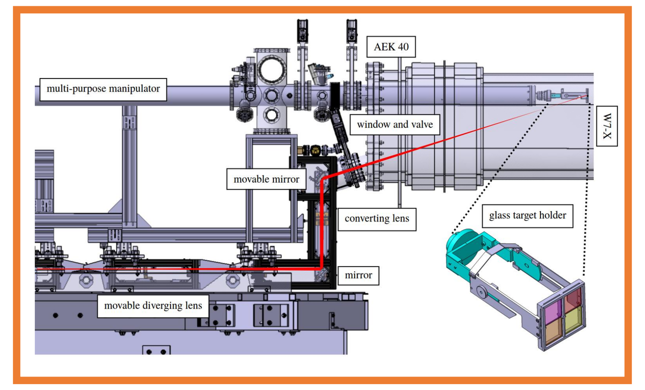

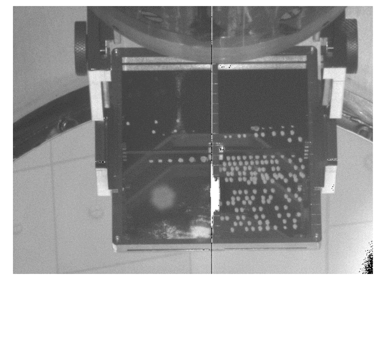

STRAHL: 1-D radial transport code

Least squares minimization of STRAHL

- STRAHL calculates the radial transport and emission of impurity ions with input of kinetic profiles and atomic data
- One dimensional means that transport and plasma parameters are at best calculated in a flux surface averaged sense
- On the user defined spatiotemporal grid STRAHL outputs an impurity ion's emissivity, $\varepsilon_{n_Z}(r, t)$, for a particular line of a particular charge state for given anomalous diffusion and convective velocity profiles.
- To match the experimentally measured emissivities, a least squares minimization is done by varying STRAHL's input anomalous diffusion and/or convective velocity parameters until a minimum is found
- STRAHL modeled spectral emissivities either need line integration or inversions to realistically match experimental signals.

STRAHL workflow: inputs & outputs

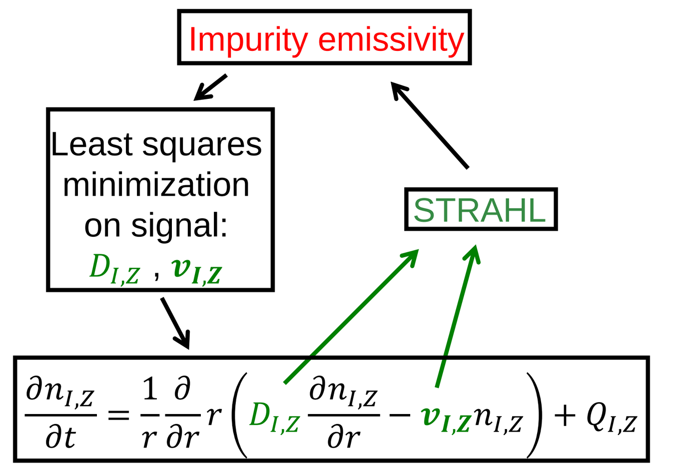

$$\frac{\partial n_{I,Z}}{\partial t} = \frac{1}{r}\frac{\partial}{\partial r} r\left(D_{I,Z}\frac{\partial n_{I,Z}}{\partial r} - v_{I,Z}n_{I,Z}\right) + Q_{I,Z}$$

Caveats: Least squares minimization of STRAHL

- Classical transport channel can be on the same order as the neoclassical channel in W7-X due to its optimization [8]
- Transport parameters are considered stationary

Example of an impurity transport experiment

20180919.043: Standard Configuration Hydrogen discharge with Fe LBO injections

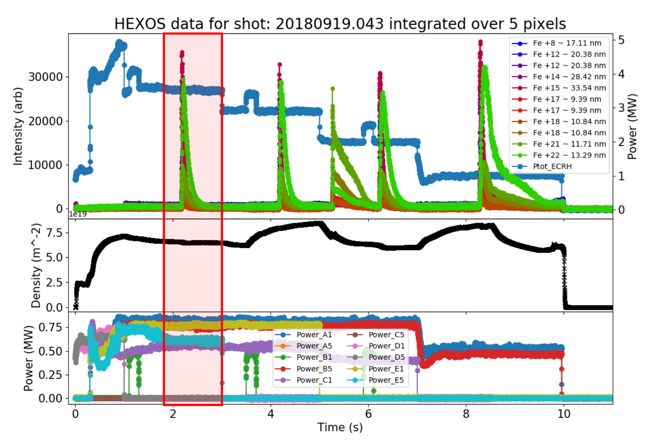

- Keeping the line-integrated density constant, ECRH total power was stepped down by turning off specific gyrotrons
- 4 Fe LBO injections starting at ~2.0 s occurred at each total power level
- Similar discharges were performed with gyrotrons at various axial heating positions from complete central heating to most off-axis heating

HEXOS signals and sightline

HR-XIS sightlines for Fe^{24+} W-line

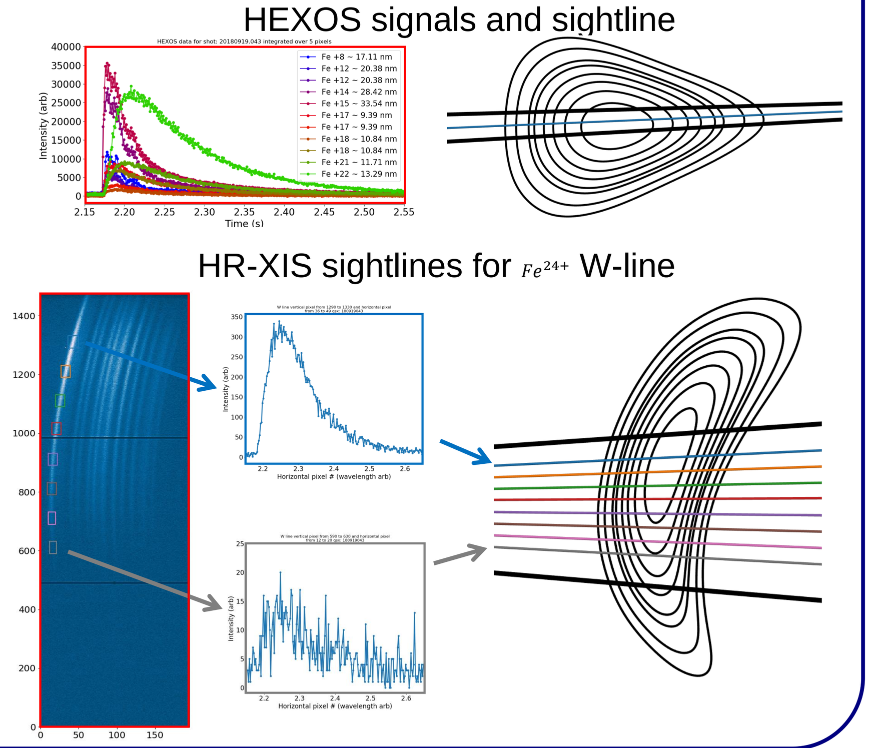

Inference of anomalous diffusion through least squares optimization over ECRH deposition variation

Overview of the on- to off-axis ECRH scan

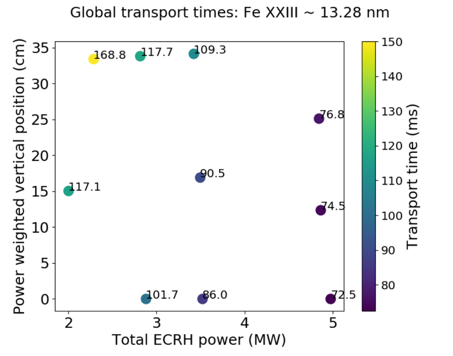

- In agreement with the OP 1.2a experiments in helium there is an increase in global impurity transport time as ECRH is moved off-axis [11]
- A fully on-axis power scan inherent to this on- to off-axis dataset demonstrates that as more ECRH power is deposited into the plasma the shorter the transport time following the known ECRH power scaling of impurity transport times

4.9 MW 3.5 MW 2.8 MW

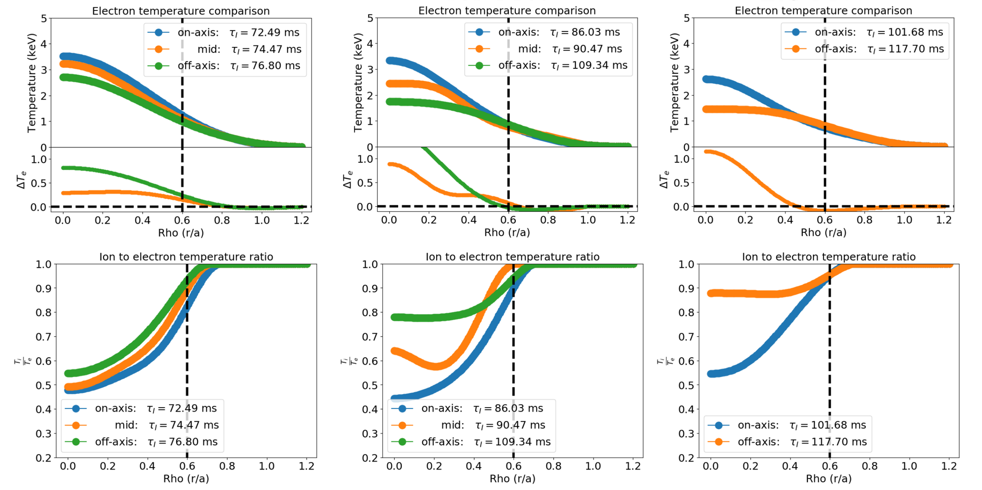

- The on- to off-axis scans performed at constant total power demonstrated that as a larger fraction of ECRH was deposited off-axis there was an increase in the $\frac{T_i}{T_e}$ ratio for $\rho \leq 0.6$ along with an enhancement of the global transport time, τ_I
- The iron impurity transport was marginally sensitive to the core electron temperature peaking. Within the on- to off-axis scans the electron temperatures in the core $\rho \leq 0.4$ were observed to change by as much as ~ 1.5 keV with a relatively small impact on the global transport time, i.e. τ_I was enhanced by at most 27% as core T_e decreased.

Classical and neoclassical transport parameters: P_{total}~3.5 MW

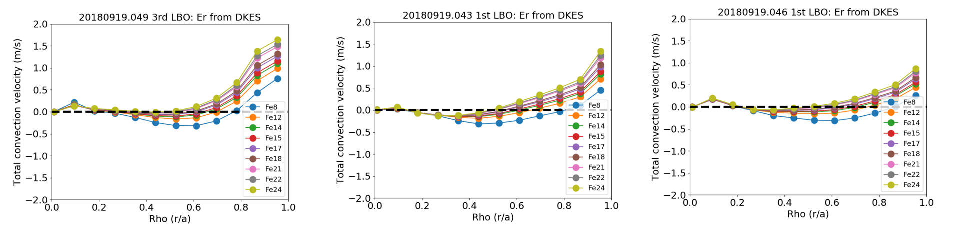

- Calculated classical and neoclassical transport parameters [9] showed minimal variation over the on- to off-axis scans despite significant core T_e peaking

Example fit: P_{total}~3.5 MW mid off-axis ECRH scenario

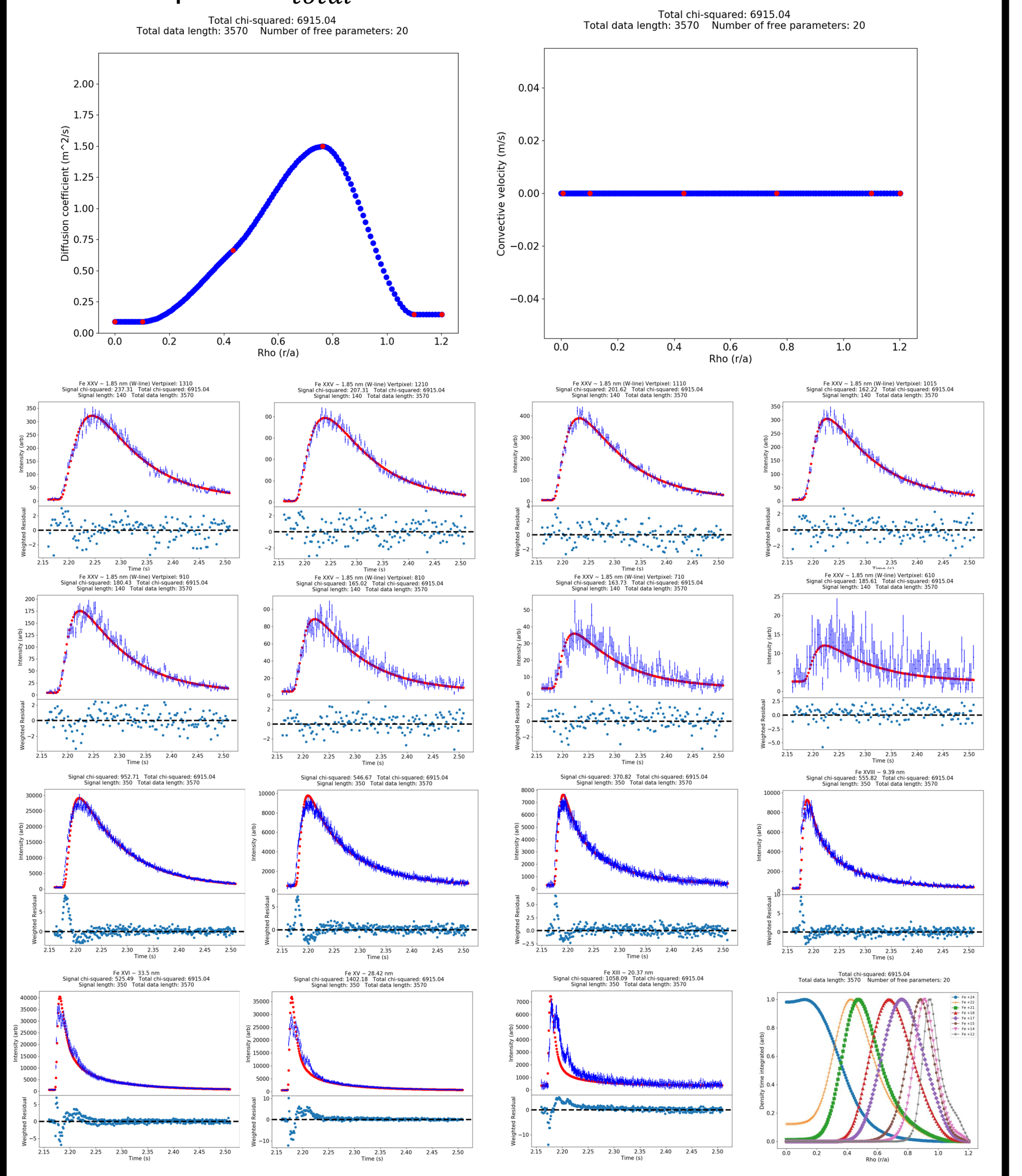

General conclusions for the inferred profiles

- Spatially resolved line radiation data is necessary for ensuring the inferred profiles are unique.
- Utilizing **only anomalous diffusive transport** within STRAHL yields good reproduction ($\chi_r^2 < 2$) of the observed iron spectral lines' time history
- Inferred anomalous diffusion values are at least an order of magnitude larger than the calculated (classical +neoclassical) diffusion as was already shown in [10] for ECRH plasmas in W7-X
- The temporal shape of the spectral lines has a stronger sensitivity to the diffusion coefficient, which is evidenced by the relatively large values of inferred convection yielding small improvements to fit (not shown)

Synthetic sensitivity studies based on realistic W7-X profiles

Goals

- Determine which model inputs, within their uncertainty levels, limit the least squares minimization from recovering the accurate transport profiles
- Understand any potential coupling between model input parameters and where possible isolate their effect on the recovery of the accurate transport profiles

Method

- Individual parameters were held at the experimentally-derived max and min values
- The residual between the true and inferred diffusion profile can be used to estimate the average error level in 4 regions

T_e profile variation

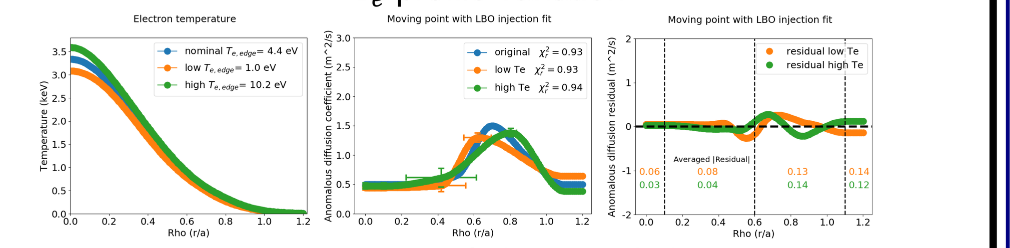

LBO temporal shape variation

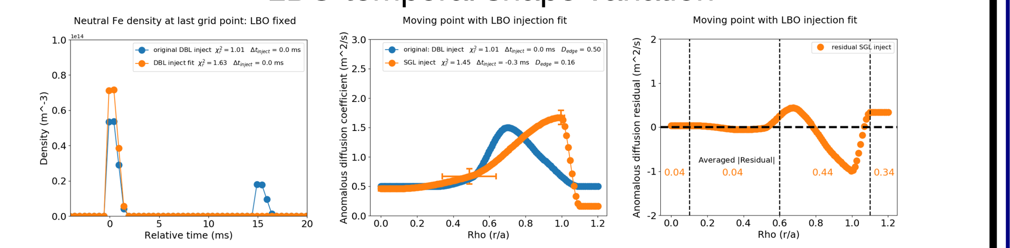

- Incorrect diagnostic timing offsets have large effects, i.e. > 0.5 $\frac{m^2}{s}$ on the accuracy of the inferred diffusion profile. **However the LBO timing offset can be determined though the least squares minimization**, while unfortunately the x-ray to VUV timing offset cannot
- **The LBO injection temporal shape characterization is critically important for accurate inference of the anomalous diffusion profile.**
- The STRAHL edge parameterization (including SOL temperatures) is important due to the indirect coupling between the LBO injection timing & the other edge parameters.
- The accurate inference of the anomalous diffusion profile is minimally effected, i.e. ~ 0.2 $\frac{m^2}{s}$ by the electron temperature profile variations within its 1-sigma uncertainties.

Total uncertainties

Uncertainty source	Parameter variations	Average of |Residual| $\left(\frac{m^2}{s}\right)$ in region ρ: 0 to .1	.1 to .6	.6 to 1.1	1.1 to 1.2
Procedural method	N.A.	0.07	0.04	0.09	0.01
Neoclassical & classical transport	50% to 200%	0.03	0.05	0.13	0.01
X-ray to VUV timing offset	±2.5 ms	0.30	0.15	0.13	0.02
LBO injection timing	±3.5 ms	5.02	2.29	2.1	0.35
LBO temporal shape	Outside a 2.5 ms window	0.04	0.04	0.14	0.19
Limiter connection length	0.5 to 25 m	0.05	0.05	0.12	0.13
Divertor connection length	200 to 300 m	0.06	0.03	0.09	0.05
T_e far SOL	1 to 16 eV	0.08	0.04	0.10	0.02
T_e core	±250 eV	0.08	0.05	0.12	0.06
T_e entire profile	(see above)	0.04	0.06	0.14	0.13
Neutral hydrogen profile	edge from 10^{14} to 10^{16} m^{-3}	0.04	0.04	0.17	0.16

Summary of least squares optimization of D & v over ECRH deposition variation

On- to off-axis ECRH scans: Fit of anomalous diffusion

4.9 MW 3.5 MW 2.8 MW

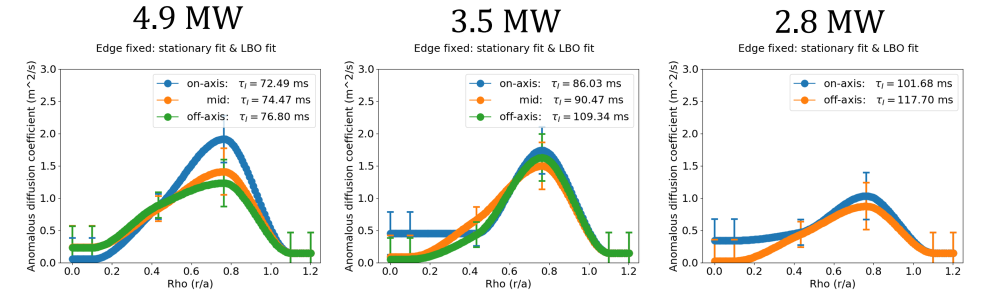

- The experimentally observed iron line emission could only be well-matched when the anomalous diffusion channel was included within the least squares inference.
- The dominance of the anomalous diffusion transport channel strongly suggests that turbulent transport is the main transport mechanism during these W7-X plasma discharges.
- The similarity of the inferred diffusion profiles are consistent with the observed similarity in the global transport times and the $\frac{T_i}{T_e}$ ratios when the synthetic studies' total uncertainties are considered
- Establishing a fixed edge anomalous diffusion value allows for consistent comparison among the inferences within an on- to off-axis ECRH dataset especially considering that at constant total ECRH power there should be minimal edge profile variations

Overview of the inherent on-axis ECRH power scan

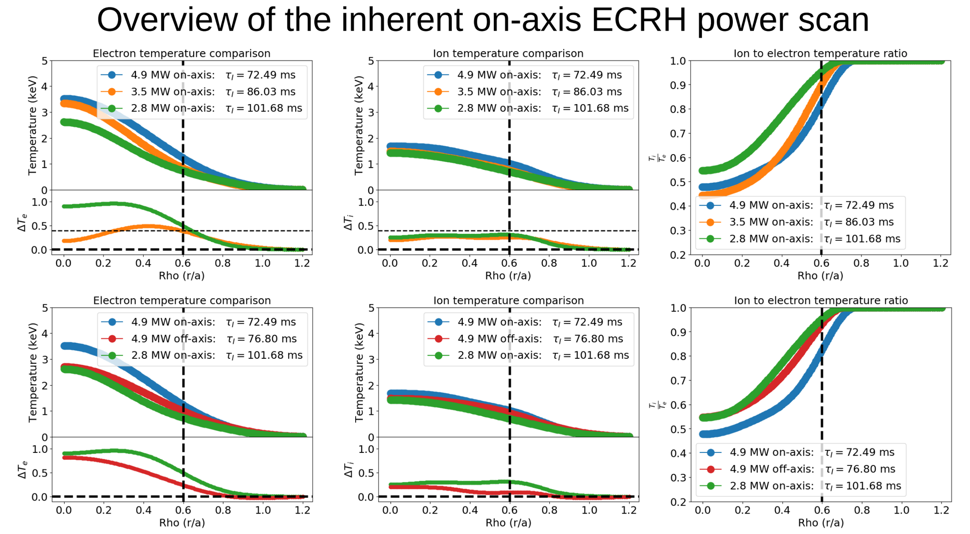

- Unlike the on- to off-axis datasets, the on-axis ECRH power scan had significant variations in the T_i and T_e profiles in the outer region of the plasma, i.e. 0.6 < ρ < 0.8
- The core T_e reduction from ~ 3.5 to 2.7 keV is nearly identical to the 4.9 MW on- to off-axis dataset, however the global transport time enhancement was substantially larger for the on-axis power scan (i.e. ~ 73 to 102 ms) than the on- to off-axis scan (i.e. ~ 73 to 77 ms)

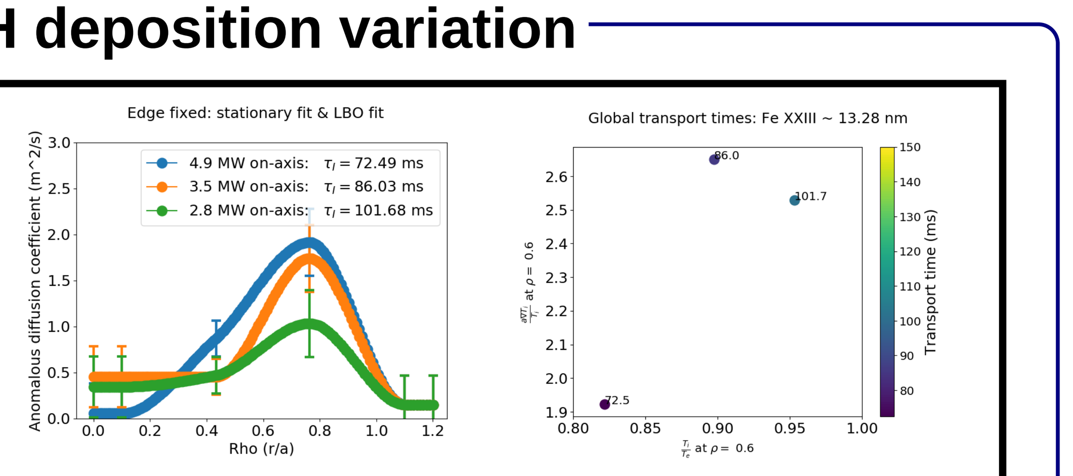

- The dominance and necessity of the anomalous diffusive flux channel is corroborated by the gyrokinetic simulations performed in [12], where irrespective of whether the turbulence was driven by ITG or TEM instabilities, it was found that the dominant impurity transport channel was ordinary, charge-independent diffusion
- Across the entire ECRH on- to off-axis dataset as either more ECRH is moved off-axis or less total ECRH power is deposited both the $\frac{T_i}{T_e}$ ratio and the τ_I increases
- The increases at the off-axis position in the $\frac{T_i}{T_e}$ ratio and the τ_I were accompanied by decreases in anomalous diffusion. This observational evidence is consistent with the suppression of ITG induced turbulent transport and the previous work done in [13]

Future work

- In order to improve the uncertainty estimations on the inferred anomalous diffusion profiles, the best way would be employing a Monte Carlo method that would generate many sets of input parameters over which a least squares minimization would be performed for every set
- Performing gyrokinetic simulations of these on- to off-axis ECRH datasets would potentially help determine the turbulent mechanism (e.g. ITG, TEM, ETG) for the observed global transport time variations.

References

[1] Th. Wegner et. al. Rev. Sci. Instrum. 89, 073505 (2018)
[2] A. Langenberg et al. Fusion Sci. Technol. 69 560-567 (2016)
[3] G. Bertschinger et al. Rev. Sci. Instrum. 75 3727 (2004)
[4] N.A. Pablant et al. 41st EPS Berlin (2014)
[5] A. Langenberg et al. Nucl. Fusion 57 086013 (2017)
[6] R. Dux et al. IPP report 10/30 (2006)
[7] M. A. Chilenski et al., Nucl. Fusion, 55, 2, 023012 (2015)
[8] S. Buller et al., J. of Plasma Phys., 85(4), 175850401 (2019)
[9] NeoTransp written by Håkan Smith (2019)
[10] B. Geiger et al, Nucl. Fusion, 59 046009 (2019)
[11] A. Langenberg et al Plasma Phys. Ctrl. Fusion 61 014030
[12] P. Helander et al Plasma Phys. Control. Fusion 60 084006
[13] Th. Wegner et al 2020 Nucl. Fusion 60 124004
[14] H. Maaßberg et al. Phys. Plasmas 7 295
[15] C. Angioni et al. Phys. Plasmas 22 102501 (2015)